Interannual variability on methane emissions in monsoon Asia derived from GOSAT and surface observations

Wang, Fenjuan

2021-02

LETTER • OPEN ACCESS

Interannual variability on methane emissions in monsoon Asia derived from GOSAT and surface observations

To cite this article: Fenjuan Wang *et al* 2021 *Environ. Res. Lett.* **16** 024040

View the article online for updates and enhancements.

ENVIRONMENTAL RESEARCH
LETTERS

LETTER

Interannual variability on methane emissions in monsoon Asia derived from GOSAT and surface observations

Fenjuan Wang[1,2], Shamil Maksyutov[1], Rajesh Janardanan[1], Aki Tsuruta[3], Akihiko Ito[1], Isamu Morino[1], Yukio Yoshida[1], Yasunori Tohjima[1], Johannes W Kaiser[4], Greet Janssens-Maenhout[5], Xin Lan[6], Ivan Mammarella[7], Jost V Lavric[8] and Tsuneo Matsunaga[1]

1 National Institute for Environmental Studies, Tsukuba, Japan
2 National Climate Center, CMA, Beijing, People's Republic of China
3 Finnish Meteorological Institute, Helsinki, Finland
4 Deutscher Wetterdienst, Offenbach, Germany
5 European Commission Joint Research Centre, Ispra, Italy
6 National Oceanic and Atmospheric Administration, Boulder, CO, United States of America
7 University of Helsinki, Helsinki, Finland
8 Max Planck Institute for Biogeochemistry, Jena, Germany

E-mail: wang.fenjuan@nies.go.jp

Abstract

In Asia, much effort is put into reducing methane (CH_4) emissions due to the region's contribution to the recent rapid global atmospheric CH_4 concentration growth. Accurate quantification of Asia's CH_4 budgets is critical for conducting global stocktake and achieving the long-term temperature goal of the Paris Agreement. In this study, we present top-down estimates of CH_4 emissions from 2009 to 2018 deduced from atmospheric observations from surface network and GOSAT satellite with the high-resolution global inverse model NIES-TM-FLEXPART-VAR. The optimized average CH_4 budgets are 63.40 ± 10.52 Tg y^{-1} from East Asia (EA), 45.20 ± 6.22 Tg y^{-1} from Southeast Asia (SEA), and 64.35 ± 9.28 Tg y^{-1} from South Asia (SA) within the 10 years. We analyzed two 5 years CH_4 emission budgets for three subregions and 13 top-emitting countries with an emission budget larger than 1 Tg y^{-1}, and interannual variabilities for these subregions. Statistically significant increasing trends in emissions are found in EA with a lower emission growth rate during 2014–2018 compared to that during 2009–2013, while trends in SEA are not significant. In contrast to the prior emission, the posterior emission shows a significant decreasing trend in SA. The flux decrease is associated with the transition from strong La Ninña (2010–2011) to strong El Ninño (2015–2016) events, which modulate the surface air temperature and rainfall patterns. The interannual variability in CH_4 flux anomalies was larger in SA compared to EA and SEA. The Southern Oscillation Index correlates strongly with interannual CH_4 flux anomalies for SA. Our findings suggest that the interannual variability in the total CH_4 flux is dominated by climate variability in SA. The contribution of climate variability driving interannual variability in natural and anthropogenic CH_4 emissions should be further quantified, especially for tropical countries. Accounting for climate variability may be necessary to improve anthropogenic emission inventories.

1. Introduction

In order to achieve the long-term temperature goal 'well below 2 °C above pre-industrial levels and pursuing efforts to limit the temperature increase to 1.5 °C above pre-industrial levels' (Schleussner *et al* 2016), a 5 year global stocktake, to summarize reported national emission inventories and compare them to the observed greenhouse gas (GHG) atmospheric trends, will take place starting 2023. The global stocktake is an essential part of the Paris Agreement for countries to take a look at how their efforts are

stacking up against the Paris Agreement temperature goal and provide inputs to parties to submit more ambitious climate pledges (Work Resources Institute 2020).

Compared to carbon dioxide (CO_2), atmospheric methane (CH_4) has a relatively shorter lifetime ($\sim$10 years) and a higher global warming potential over 100 years, which makes it a suitable target for implementing rapid and achievable mitigation strategies (Dlugokencky *et al* 2011, Nisbet *et al* 2020). The concentration level of CH_4 in the atmosphere is over 150% higher than pre-industrial times (i.e. year 1750), and the current sharp rise of CH_4 concentration makes it as the key GHG threatening achievement of the Paris Agreement mitigation targets (Bousquet *et al* 2006, Nisbet *et al* 2019). The exact reasons for the CH_4 concentration accelerated are so far not well understood, in relevance to anthropogenic and natural emission activities, climate change, and tropospheric oxidant changes (Ghosh *et al* 2015, Saunois *et al* 2016b, Nisbet *et al* 2019, Turner *et al* 2019). Greenhouse gas Observing SATellite (GOSAT) observations detected significant enhancements of column-averaged dry-air mole fraction of methane (XCH_4) in Asia in the course of its operation since 2009 (Kivimaki *et al* 2019). The CH_4 concentration showed significantly increasing trends across China, which would bring a potential rise in surface temperature response over China (Wu *et al* 2019). Asia, with 60% of the population in the world, shares around 30% of global total CH_4 emissions, and around 40% of global anthropogenic emissions (Saunois *et al* 2016a). Previous studies reported increasing CH_4 emission in Asia during 2000–2012 due to increases of population, coal and natural gas consumption, paddy fields, and livestock (Patra *et al* 2016, Ito *et al* 2019, Saunois *et al* 2020). The observed CH_4 increase in Asia is attributed to emissions from big emitting countries with rapid economic growth (Bergamaschi *et al* 2013, Ito *et al* 2019). Asia, with 87% of the global rice paddy area and 90% of rice production over the world, is globally the main contributor to CH_4 emissions from agriculture (FAOSTAT 2017). As recent studies suggest that the paddy area was decreasing in Asia since 2007 (Zhang *et al* 2020a), other possible drivers should be addressed to explain the recent global CH_4 increase. CH_4 mitigation in the frame of the Paris Agreement, also requires a sound analysis of past emissions since the determination of national emission reduction targets and policies is directly affected by CH_4 emission budgets produced by individual countries (Feng *et al* 2017). Top-down methods are efficient tools for evaluation of emissions, as in the bottom-up inventories remain large uncertainties (Kirschke *et al* 2013, Lyon *et al* 2015, Peischl *et al* 2016, Peng *et al* 2016, Saunois *et al* 2016a, 2017), especially in non-CO_2 emission inventories the uncertainty around 50% at the higher end (Kirschke *et al* 2013, Wang *et al* 2018, Saunois *et al* 2020). Due

to the improvement of inverse modeling and various observations available (Jacob *et al* 2016, Houweling *et al* 2017), especially the GOSAT's 10 year record of CH_4 retrievals (Parker *et al* 2020), there is an increasing number of top-down GHG budget estimations by inverse models (e.g. Brown 1993, Bergamaschi *et al* 2010, 2018, Fraser *et al* 2013, Maksyutov *et al* 2013, Miller *et al* 2013, 2019, Alexe *et al* 2015, Turner *et al* 2015, Tan *et al* 2016, Sheng *et al* 2018a, 2018b).

In this paper, we estimated top-down CH_4 emissions for monsoon Asia at the country scale for 2009–2018 by a global high-resolution ($0.1° \times 0.1°$) inverse model using surface observations and GOSAT retrievals. We analyzed the spatiotemporal variations of anthropogenic and natural CH_4 fluxes in East, Southeast and South Asia during 2009–2018, took stock of two 5 year (2009–2013 and 2014–2018) emission budgets of top-emitting countries in Asia, and explored aspects that should be taken into account for coming global stocktake and further guidelines for the nationally determined contributions to emission reduction in Asia.

2. Data and method

2.1. Inverse model

To estimate the top-down CH_4 emissions, we used the joint Eulerian three-dimensional transport model National Institute for Environmental Studies Transport Model (NIES-TM) coupled with a Lagrangian particle dispersion model named FLEXible PARTicle dispersion model (FLEXPART) (Ganshin *et al* 2012, Belikov *et al* 2016). The coupled model NTFVAR combines NIES-TM v08.1i with a horizontal resolution of 2.5° and 32 hybrid-isentropic vertical levels (Belikov *et al* 2013) and FLEXPART model v.8.0 (Stohl *et al* 2005). The design of the inverse modeling system NTFVAR and the inverse method were described in details by Maksyutov *et al* (2020). The model adjoint, performance test and validation were described by Belikov *et al* (2016). The inverse modeling problem is formulated and solved to find the optimal value of *x*—vectors of corrections to prior fluxes at the minimum of the cost function $J(x)$ in equation (1):

$$J(x) = \frac{1}{2}(H \cdot x - r)^T \cdot R^{-1} \cdot (H \cdot x - r) + \frac{1}{2}x^T \cdot B^{-1} \cdot x$$

(1)

where *r* is the residual (the difference between the observed concentration and the forward simulation made with prior fluxes without correction), *R* is the covariance matrix of observations, and *B* is the covariance matrix of fluxes. *H* is a matrix representing transport model. Flux corrections were estimated independently for two categories of emissions (i.e. anthropogenic and natural). Variational optimization was applied to obtain flux corrections as two sets of scaling factors to prior uncertainty fields on

a monthly basis at a 0.1° × 0.1° resolution separately for anthropogenic and natural wetland emissions with bi-weekly time steps. The inverse model operates at the resolution of coupled transport model of 0.1° × 0.1° and applies spatial flux covariance length of 500 km. Sensitivity tests for the inversion setup have been performed using randomly perturbed observations and perturbed fluxes for different regions (Wang *et al* 2019), and inversion results have been validated against aircraft measurement data, which were not used in the inverse simulations as described in Janardanan *et al* (2020). More details about the model setup and initial condition test are described in supplementary material (available online at stacks.iop.org/ERL/16/024040/mmedia).

2.2. Data sources

Prior CH_4 fluxes used in the model include anthropogenic emissions, natural emissions from wetlands, soil sink, emissions from biomass burning and other natural sources from the ocean, geological reservoirs and termites. Annual anthropogenic emissions were taken from the latest Emissions Database for Global Atmospheric Research (EDGAR v5.0). Monthly variation of anthropogenic emissions was incorporated based on the monthly emissions by EDGAR for the year 2015. Beyond 2015, we used the report from PBL Netherlands Environmental Assessment Agency (Olivier and Peters 2018) to extend EDGAR values of 2015 using equation (2), where *t* is year from 2016 to 2018:

$$E_{\mathrm{UNFCCC}}(t) = E_{\mathrm{UNFCCC}}(2015) \times \frac{\mathrm{PBL}_{\mathrm{CH4}}(t)}{\mathrm{PBL}_{\mathrm{CH4}}(2015)}. \tag{2}$$

Wetlands emissions (Cao mechanism (Cao *et al* 1996)) and soil sink (Curry mechanism (Curry 2007)) were from improved VISIT (Vegetation Integrative SImulator for Trace gases) model simulations (Ito and Inatomi 2012). Biomass burning emissions were from the daily GFASv1.2 (Global Fire Assimilation System) (Kaiser *et al* 2012). The oceanic, geological, and termite emissions were also included (Fung *et al* 1991, Lambert and Schmidt 1993). The uncertainties of the prior CH_4 fluxes were set for 30% of EDGAR and 50% of VISIT in the inversion.

From GOSAT, we used in our inversion the XCH_4 data from the thermal and near-infrared sensor for carbon observation-Fourier transform spectrometer. The GOSAT data were corrected as described in the supplementary material. In addition to the GOSAT retrievals (NIES, Level 2 retrievals, v.02.81) (Yoshida *et al* 2013), we used ground-based atmospheric CH_4 observations from the World Data Centre for Greenhouse Gases (WDCGG) in the inversions (Dlugokencky *et al* 2019), uncertainties were set for GOSAT and each site according to the observations (for more details refer to Wang *et al* (2019) and

sites map are in figure S3 in supplementary material). The meteorological data such as three-dimensional wind fields, temperature, and humidity at a temporal resolution of 6 h used for the transport model were obtained from the Japanese Meteorological Agency Climate Data Assimilation System and the Japanese 55 year Reanalysis (JRA-55) (Onogi *et al* 2007, Kobayashi *et al* 2015).

3. Results and discussion

3.1. Regional CH_4 fluxes and spatial distribution

There are 27 countries included in the study area, which we divided into three subregions: East Asia (EA), South Asia (SA), and Southeast Asia (SEA).

Figure 1 shows the spatial distribution of the average 2009–2018 posterior natural and anthropogenic emissions and flux correction scales. The flux correction scales are represented by the mean ratios of annual mean flux corrections to the multi-annual mean prior emissions (Wang *et al* 2019). A notable decrease of 10%–20% in posterior anthropogenic fluxes is shown in the east of China, Korea, and Japan, whereas there are significant upwards corrections for natural emissions in Tibet of China and northeast of India. The total posterior emission of 171.33 ± 25.90 Tg y^{-1} over the study area for 2009–2018 is 4.31 Tg y^{-1} lower than the prior estimate (figure 2). The posterior anthropogenic emission is dominant in the area accounting for 133.56 Tg y^{-1}, 4.8% lower than the prior estimate. Hotspots of anthropogenic CH_4 emissions are distributed mostly in the densely populated city clusters in eastern China, northern India, southern Malaysia, south of Vietnam and Thailand. Emissions in these hotspots are driven by anthropogenic sources such as livestock, rice cultivation, coal exploitation, landfill, and waste. In northern China, where coal, oil and natural gas are mostly produced in the country, CH_4 emissions are mainly from these sources. North-eastern China has high CH_4 emissions from rice paddy. Southern and central China have high CH_4 emissions from rice paddy, waste treatment, and fossil fuel combustion (Zhang and Chen 2014, Peng *et al* 2016). Rice paddy and livestock are main anthropogenic sources in India and SEA countries besides emissions from natural gas and coal. (MoEFCC 2018, Scarpelli *et al* 2020). The posterior natural emission of 37.76 Tg y^{-1} is 6.7% higher than the prior estimate. Natural emissions are prominent in Tibet and Yangtze river basin in China, northeast India, southeast Asian countries such as Laos, Cambodia, where wetlands are main natural source. Particularly the Tibet region has high CH_4 emissions from wetlands.

The optimized average CH_4 budgets over 2009–2018 are 63.40 ± 10.52 Tg y^{-1} from EA, 45.20 ± 6.22 Tg y^{-1} from SEA, and 64.35 ± 9.28 Tg y^{-1} from SA. The difference between the
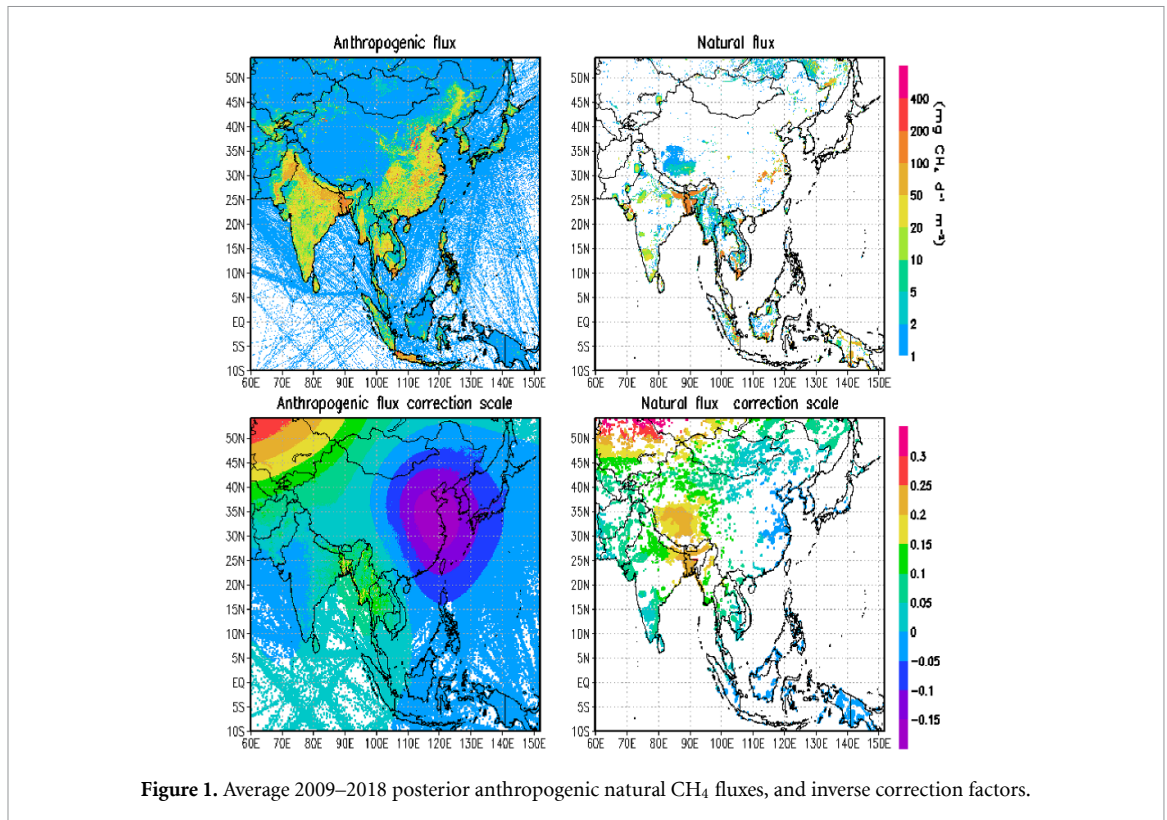
Figure 1. Average 2009–2018 posterior anthropogenic natural CH$_4$ fluxes, and inverse correction factors.
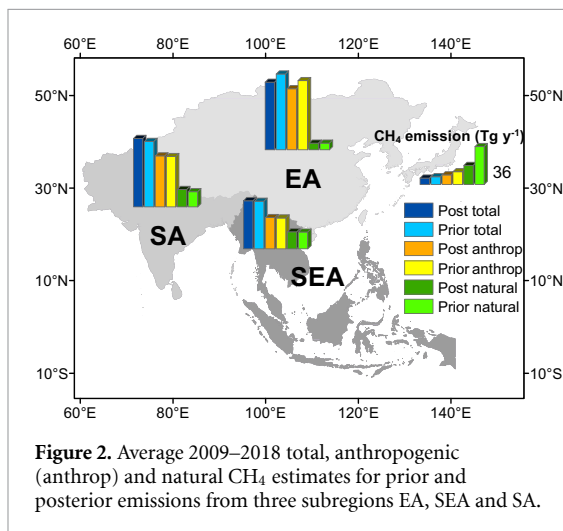

Figure 2. Average 2009–2018 total, anthropogenic (anthrop) and natural CH$_4$ estimates for prior and posterior emissions from three subregions EA, SEA and SA.

prior estimates and the posterior estimates are within the model uncertainty range. The estimate of CH$_4$ emissions from SEA in this study is consistent with the estimate (43.5 ± 3.2) of Fraser *et al* (2013) and the estimate (41.5 ± 6.8) of Tan *et al* (2016). Note the study domain does not totally match that of this study and the periods of the estimations are different, which would cause the differences.

For evaluation of the results from our inversion, we conducted a comparison of the modeled CH$_4$ concentrations using prior and posterior emissions and the measured concentrations. The estimation was evaluated by comparing the simulated and observed measurements at 13 surface sites in the study area (table S1 in supplementary material). The estimates

with posterior emissions show decreased bias, root mean square error (RMSE) and improved correlations between observed and simulated concentrations, which indicates that our inverse model obtains optimized emissions that fit to the observations better. The improvement of our inversion optimizations is comparable to other studies or even better with lower RMSE (e.g. Alexe *et al* 2015, Zhang *et al* 2020b).

3.2. CH$_4$ budgets and trends in 2009–2013 and 2014–2018

According to the Paris Agreement, the global stocktake will be conducted in 2023, and a 5 year review will be taken regularly (Work Resources Institute 2020). National reports to the UNFCCC are currently rare for most Asian countries. Only Japan and Korea submitted national inventories yearly up to 2018; China reported values of 2010, 2012, and 2014; India, Pakistan, Vietnam, Thailand, and Malaysia reported only once during the study period 2009–2018 (UNFCCC 2020). Here, we evaluate the last two 5 year CH$_4$ emission budgets in monsoon Asia for countries that emit more than 1 Tg y^{-1} using top-down inverse estimates (table 1). These 13 countries emit more than 97% of the total CH$_4$ emissions in the study area, and anthropogenic emissions are dominant in most countries except Bangladesh and Cambodia. The posterior total emissions stay stable from the first 5 year period to the second, while the prior total emissions show a 4% increase in the whole study area. The optimized total emissions for China, Japan, and South Korea show larger increases compared to

Table 1. Five-yearly prior and posterior CH$_4$ emissions from countries with annual emission budget larger than 1 Tg in monsoon Asia.

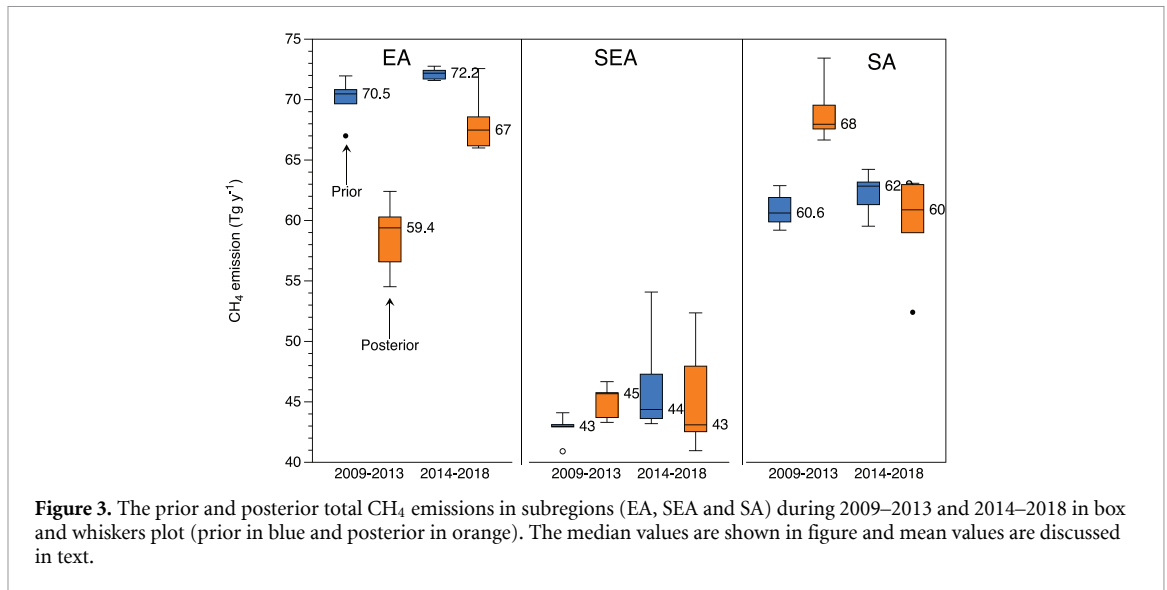|	Prior (Tg y^{-1})			Posterior (Tg y^{-1})				
	2009–2013	2014–2018	Change (%)	2009–2013	2014–2018	Change (%)	Uncertainty (Tg y^{-1})	Posterior anthropogenic (%) 2009–2018
Total	172.02	179.28	4.22	170.99	171.69	0.41	25.71	78
China	64.00	66.16	3.39	53.72	62.16	15.72	8.63	90
India	41.56	42.49	2.24	46.33	40.11	−13.43	5.33	76
Indonesia	17.63	21.30	20.80	17.72	20.53	15.83	2.52	62
Bangladesh	8.99	8.41	−6.54	11.35	8.93	−21.30	1.70	51
Pakistan	7.55	8.45	11.91	8.22	7.83	−4.70	1.04	93
Vietnam	6.09	6.38	4.66	6.43	6.11	−5.00	1.09	67
Thailand	5.78	5.37	−7.18	6.51	5.43	−16.55	1.00	77
Myanmar	5.28	5.22	−1.26	6.13	5.37	−12.36	0.84	62
Philippines	2.95	3.09	4.76	2.88	2.91	0.84	0.44	91
Cambodia	2.24	2.28	1.67	2.42	2.23	−7.97	0.42	44
Japan	2.23	2.10	−5.61	1.84	2.15	16.87	0.20	93
Nepal	1.27	1.31	2.96	1.48	1.28	−13.50	0.19	90
South Korea	1.37	1.34	−2.21	0.99	1.32	33.55	0.21	97

Figure 3. The prior and posterior total CH_4 emissions in subregions (EA, SEA and SA) during 2009–2013 and 2014–2018 in box and whiskers plot (prior in blue and posterior in orange). The median values are shown in figure and mean values are discussed in text.
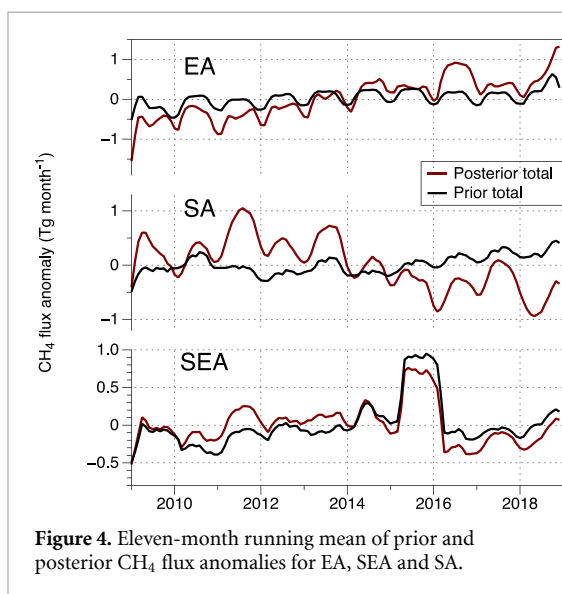

Figure 4. Eleven-month running mean of prior and posterior CH_4 flux anomalies for EA, SEA and SA.

2015 is also lower than model estimates (table 1). The trends reveal geographical features; thus, we further explored the difference between the aggregated emissions for two 5 year periods for three subregions. Figure 3 shows prior and posterior emissions during two 5 year periods from subregions. In the first and second 5 year periods, the mean posterior emissions in EA are 58.64 Tg y^{-1} and 68.16 Tg y^{-1}, both lower by 16% and 6% than the mean prior emissions (69.98 Tg y^{-1}, 72.13 Tg y^{-1}), respectively. The mean posterior emissions in SEA and SA are higher than the mean prior emissions by 5% and 13% during 2009–2013, but lower by 2% and 4% during 2014–2018. The mean posterior emission in SA decreases from 69 Tg y^{-1} to 59.7 Tg y^{-1} by 16% from the first 5 year period to the second 5 year period. The mean posterior estimates in SEA are similar around 45 Tg y^{-1} in the two 5 year periods.

3.3. Interannual flux variability

Ten years of monthly fluxes of prior and posterior estimates were aggregated for three subregions to investigate the interannual flux variabilities. Figure 4 shows the anomalies for prior and posterior total emissions in subregions EA, SA and SEA. The anomalies are constructed by subtracting the long-term monthly mean from the raw time series and constructing the 11 month running mean on the resultant time series. The long-term gradual trend was excluded by using anomalies. The amplitudes of anomalies coincide with the seasonal variability in three regions with maximum emissions in summer and minimum in winter. The prior anomalies of three regions show less variability compared to the posterior anomalies. The posterior anomaly of EA shows notable positive excursions in 2016 and 2018. The posterior anomaly of SA shows relatively larger variability with the largest positive excursion in 2011 and negative anomalies in 2016 and 2018. The posterior

the prior estimates since the posterior emissions during the first 5 year period are lower than the prior emissions. The national report to UNFCCC of China is around 55 Tg y^{-1} during 2010–2014, closer to the posterior estimates (53.72 Tg y^{-1}, 62.16 Tg y^{-1}) than to the prior estimates (64.00 Tg y^{-1}, 66.16 Tg y^{-1}). The Japan national report to the UNFCCC shows values between 1.2 and 1.4 Tg y^{-1}, lower than both prior (2.13 Tg y^{-1}, 2.10 Tg y^{-1}) and posterior (1.84 Tg y^{-1}, 2.15 Tg y^{-1}). The optimized total emissions in other countries show less increase compared to the prior estimates, in which India, Pakistan, Thailand, Bangladesh, and Myanmar obtain higher optimized emissions during the first 5 year period compared to the prior emissions. The model estimates for India aresimilar to the studies by Saunois *et al* (2016a), Miller *et al* (2019), but higher than the study of Ganesan *et al* (2017) and the Indian national report to the UNFCCC (of 19.78 Tg y^{-1} in 2010). The national report of Pakistan with 5.55 Tg y^{-1} in
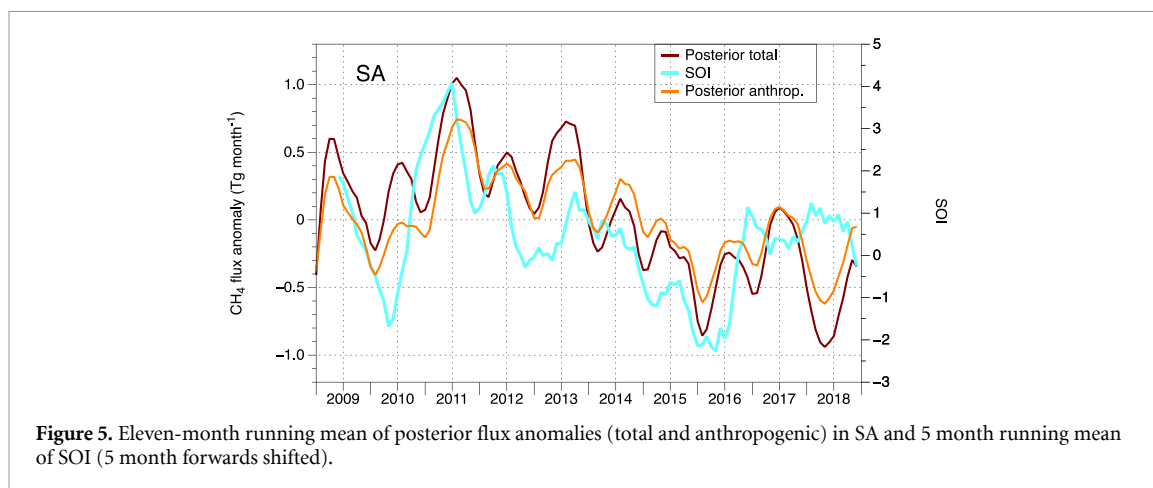
Figure 5. Eleven-month running mean of posterior flux anomalies (total and anthropogenic) in SA and 5 month running mean of SOI (5 month forwards shifted).

anomaly of SEA shows relatively smaller variability except for an anomalous positive peak in 2015 coherence with prior anomaly due to the intensive fires in Indonesia that year, which emitted globally significant quantities of GHGs to the atmosphere, and significant enhancement of CH_4 total column values were observed by GOSAT (Parker *et al* 2016).

We investigated the trends in flux anomalies using the non-parametric Mann–Kendall approach (Hirsch *et al* 1982). The null hypothesis of trend test is no significant trend existing in a flux series, and a trend in flux series is considered 'significant' if the test probability $P \leqslant 0.05$. The results show statistically significant increasing trends in prior anomalies of EA, SEA, SA. The posterior anomalies show a statistically significant increasing trend in EA and a decreasing trend in SA. There is no statistically significant trend detected in the posterior anomaly of SEA. The anticorrelation between increasing prior flux and decreasing posterior flux from SA is not noticed before and causes interest to probe.

3.4. Connection between CH_4 flux variability and SOI

According to the EDGAR v5.0 estimate, the anthropogenic CH_4 emission sources in SA include mainly livestock (47%), rice (22%), waste (16%), and energy (15%), and the CH_4 emissions from livestock, rice and waste sectors keep rising in the study period due to increasing production by ruminants, paddy field harvest areas and waste, etc. We found in this study that the anomaly of anthropogenic emission in SA has a similar trend and variation with the anomaly of total emission in SA ($r = 0.93$ using Pearson's correlation test) (figure 5). We probed into the possible climate factors that might drive the flux variabilities, which are not calculated in the activity-based bottom-up estimates. The dominant interannual variability of the global climate system is ENSO (El Ninño-Southern Oscillation) (Trenberth *et al* 1998, Messie and Chavez 2011), which plays a central role in seasonal to decadal global climate and impacts

temperature and precipitation in its whole lifecycle. In Southern Asia, surface air temperature and precipitation can be significantly modulated by ENSO (Lin and Qian 2019, Gehlot *et al* 2020). We investigated the connection between the smoothed posterior anomaly of SA emissions and the smoothed Southern Oscillation Index (SOI). The SOI is a measure of the intensity or strength of the Walker Circulation and the SOI is defined as the difference in surface air pressure between Tahiti and Darwin (Troup 1965). Prolonged periods of negative (positive) SOI values coincide with abnormally warm (cold) ocean waters across the eastern tropical Pacific typical of El Ninño (La Ninña) episodes (Wolter and Timlin 2011). A strong La Ninña event occurred in 2010–2011, a moderate La Ninña event in 2011–2012, and a very strong El Ninño event occurred in 2015–2016 (figure 5) (SOI data accessed from (Australia Meteorology Bureau 2020)). The positive flux anomalies in both SA and SEA in 2011 (figure 4) respond to the La Ninña event of 2010–2011. The negative flux anomaly of SA responds to the strong El Ninño event of 2015–2016.

The trends of SOI (5 month forwards shift) and the flux anomalies in SA are in good agreement (figure 5). We used the Pearson test to examine the correlation and good correlations were found between SOI and the total flux and the anthropogenic flux anomalies with $r = 0.6$ (p-value $= 2.1 \times 10^{-9}$) and $r = 0.5$ (p-value $= 7.2 \times 10^{-10}$), respectively. The decrease of CH_4 fluxes from 2010 to 2016 corresponds to a cold-to-warm transition from a strong La Ninña in 2010 to a strong El Ninño in 2016 in SA. Recently, Sun *et al* (2020) conducted long-term field CH_4 flux measurement in the Yangtze River delta, China, and found that higher temperature and less rainfall in 2013 induced CH_4 emissions increase from rice paddy by 58%–294%, while rice grain yield did not increase and straw biomass increased by 15%–40% compared to other years. A previous study also found that Indian rice production dropped by 7% during El Ninño events (Selvaraju 2003). Another

study found that rising temperature results in an increase in CH_4 production per unit of livestock products (Broucek 2015). The source for CH_4 production by ruminant enteric fermentation is a dietary carbohydrate, which influences the rate of fermentation, rate of rumen passage, and animal intake, contributing around 90% CH_4 emissions of livestock. In a high-temperature environment, the contents of the cell wall, acid detergent fiber, and lignin tend to increase, causing lower digestibility of feed and higher energy loss, which results in an increase in CH_4 production per unit of product through the decrease in the efficiency of animal production in tropics. Forage quality increase with decreasing temperatures induces a decrease of enteric CH_4 production (Lee *et al* 2017). With a 70% of CH_4 emissions from rice paddy and livestock, the SA flux variability is closely associated with climate variability, which might be not accounted for in the prior estimates.

4. Conclusions

This study presents the first detailed CH_4 budgets in East, Southeast, and South Asia inferred from a decade of satellite and ground-based atmospheric observations from 2009 to 2018 on a country scale. We used the global high-resolution inverse model NIES-TM-FLEXPART-VAR to optimize prior anthropogenic emissions from EDGAR v5.0, wetland emissions from VISIT model, and biomass emissions from GFASv1.2. The inverse corrections vary geographically, we found evident downwards anthropogenic emission corrections in eastern China, Korea and Japan, and upwards natural emission corrections in Tibet of China and northeast of India. The optimized average CH_4 budgets are 63.40 Tg y^{-1} from EA, 45.20 Tg y^{-1} from SEA, and 64.35 Tg y^{-1} from SA in a ten-year period. Emission budgets are estimated in two 5 year periods 2009–2013, 2014–2018 for countries with an emission budget of more than 1 Tg yr^{-1} (13 countries).

We compared the optimized CH_4 flux variations with the prior inventories. The prior estimates show significant increasing trends in EA, SEA, and SA, while posterior estimates release trends with geographical features. In EA the increasing trend is statistically significant, and in SEA no significant trend is singled out. The posterior emission in SA releases a significant decreasing trend on the contrary to the prior emission, and the flux is more variable compared to that in EA and SEA. We further probed the opposite trends found in prior and posterior emissions in SA and found that the SOI correlates well with the interannual anomalies of CH_4 flux. The flux decrease is associated with the transition of strong La Ninña (2010–2011) to strong El Ninño (2015–2016) events and its accompanying effect of the Asian Monsoon system, which drives the patterns of temperature and rainfall. Recent field studies as discussed in

section 3.4 found that decreasing temperature induce decreasing CH_4 fluxes from the paddy field, livestock, and waste, and these climate-CH_4 feedbacks explaining the decreasing trend in the posterior flux anomalies in SA may not be calculated in the prior flux estimates. The abnormally low anthropogenic emissions in SA and high fire emissions in SEA were found related to the strong El Ninño event in 2015.

Our results also demonstrate the importance of the information about interannual variations in CH_4 fluxes in Asia is strongly influenced by ENSO climate variations. Strong negative anomalies in CH_4 fluxes occur during El Niño events in SA and notable positive anomalies in CH_4 fluxes are detected during La Ninña events in SA and SEA. Climate variability drives agriculture and wastes emission changes, a recent decrease of CH_4 emission in SA more likely due to climate variability (e.g. ENSO) rather than production yield decrease. Climate variability affects CH_4 emissions from paddy fields and livestock should be considered in the coming global stocktake under the Paris Agreement, in order to increase the accuracy, better explain changes in CH_4 budgets between 5 year stocktake periods. Accordingly, more studies are required to address climate–anthropogenic CH_4 feedbacks and to quantify the contribution of climate variability to interannual variabilities in CH_4 fluxes.

Conflict of interest

The authors declare no conflicts of interest.

ORCID iDs

Fenjuan Wang ⦿ https://orcid.org/0000-0003-3417-6170
Shamil Maksyutov ⦿ https://orcid.org/0000-0002-1200-9577
Aki Tsuruta ⦿ https://orcid.org/0000-0002-9197-3005
Akihiko Ito ⦿ https://orcid.org/0000-0001-5265-0791
Johannes W Kaiser ⦿ https://orcid.org/0000-0003-3696-9123

Jost V Lavric ⬤ https://orcid.org/0000-0003-3610-9078

References

Alexe M *et al* 2015 Inverse modelling of CH$_4$ emissions for 2010–2011 using different satellite retrieval products from GOSAT and SCIAMACHY *Atmos. Chem. Phys.* **15** 113–33

Australia Meteorology Bureau 2020 Southern Oscillation Index (SOI) since 1876 (Australia Government, Bureau of Meteorology) (available at: www.bom.gov.au/climate/current/soi2.shtml)

Belikov D *et al* 2013 Simulations of column-averaged CO$_2$ and CH$_4$ using the NIES TM with a hybrid sigma-isentropic (sigma-theta) vertical coordinate *Atmos. Chem. Phys.* **13** 1713–32

Belikov D, Maksyutov S, Yaremchuk A, Ganshin A, Kaminski T, Blessing S, Sasakawa M, Gomez-Pelaez A and Starchenko A 2016 Adjoint of the global Eulerian-Lagrangian coupled atmospheric transport model (A-GELCA v1.0): development and validation *Geosci. Model Dev.* **9** 749–64

Bergamaschi P *et al* 2010 Inverse modeling of European CH$_4$ emissions 2001–2006 *J. Geophys. Res.* **115** D22309

Bergamaschi P *et al* 2013 Atmospheric CH$_4$ in the first decade of the 21st century: inverse modeling analysis using SCIAMACHY satellite retrievals an^{++}-d NOAA surface measurements *J. Geophys. Res.* **118** 7350–69

Bergamaschi P *et al* 2018 Inverse modelling of European CH$_4$ emissions during 2006–2012 using different inverse models and reassessed atmospheric observations *Atmos. Chem. Phys.* **18** 901–20

Bousquet P *et al* 2006 Contribution of anthropogenic and natural sources to atmospheric methane variability *Nature* **443** 439–43

Broucek J 2015 Methane yield from cattle, sheep, and goats housing with emphasis on emission factors: a review *Slovak J. Anim. Sci.* **48** 122–39

Brown M 1993 Deduction of emissions of source gases using an objective inversion algorithm and a chemical-transport model *J. Geophys. Res.* **98** 12639–60

Cao M, Marshall S and Gregson K 1996 Global carbon exchange and methane emissions from natural wetlands: application of a process-based model *J. Geophys. Res.* **101** 14399–414

Curry C 2007 Modeling the soil consumption of atmospheric methane at the global scale *Glob. Biogeochem. Cycles* **21** GB4012

Dlugokencky E, Crotwell A, Mund JW and Thoning KW 2019 Atmospheric Methane Dry Air Mole Fractions from the NOAA GML Carbon Cycle Cooperative Global Air Sampling Network, 1983-2018 *Bremerhaven, NOAA* **2019–7**

Dlugokencky E, Nisbet E, Fisher R and Lowry D 2011 Global atmospheric methane: budget, changes and dangers *Phil. Trans. R. Soc. A* **369** 2058–72

FAOSTAT 2017 Paris Rulebook: global stocktake (Food and Agriculture Organization of the United Nations) (available at: www.fao.org/faostat/en/#data/QC/visualize)

Feng T, Yang Y, Xie S, Dong J and Ding L 2017 Economic drivers of greenhouse gas emissions in China *Renewable Sustainable Energy Rev.* **78** 996–1006

Fraser A *et al* 2013 Estimating regional methane surface fluxes: the relative importance of surface and GOSAT mole fraction measurements *Atmos. Chem. Phys.* **13** 5697–713

Fung I, John J, Lerner J, Matthews E, Ppather M, Steele L and Fraser P 1991 3-Dimensional model synthesis of the global methane cycle *J. Geophys. Res.* **96** 13033–65

Ganesan A L *et al* 2017 Atmospheric observations show accurate reporting and little growth in India's methane emissions *Nat. Commun.* **8** 836

Ganshin A *et al* 2012 A global coupled Eulerian-Lagrangian model and 1 × 1 km CO2 surface flux dataset for high-resolution atmospheric CO$_2$ transport simulations *Geosci. Model Dev.* **5** 231–43

Gehlot L K, Jibhakate S M, Sharma P J, Patel P L and Timbadiya P V 2020 Spatio-temporal variability of rainfall indices and their teleconnections with El Niño-Southern oscillation for Tapi Basin, India *Asia-Pac. J. Atmos. Sci.* **57** 210

Ghosh A *et al* 2015 Variations in global methane sources and sinks during 1910–2010 *Atmos. Chem. Phys.* **15** 2595–612

Hirsch R, Slack J and Smith R 1982 Techniques of trend analysis for monthly water-quality data *Water Resour. Res.* **18** 107–21

Houweling S, Bergamaschi P, Chevallier F, Heimann M, Kaminski T, Krol M, Michalak A and Patra P 2017 Global inverse modeling of CH$_4$ sources and sinks: an overview of methods *Atmos. Chem. Phys.* **17** 235–56

Ito A and Inatomi M 2012 Use of a process-based model for assessing the methane budgets of global terrestrial ecosystems and evaluation of uncertainty *Biogeosciences* **9** 759–73

Ito A, Tohjima Y, Saito T, Umezawa T, Hajima T, Hirata R, Saito M and Terao Y 2019 Methane budget of East Asia, 1990–2015: a bottom-up evaluation *Sci. Total Environ.* **676** 40–52

Jacob D, Turner A, Maasakkers J, Sheng J, Sun K, Liu X, Chance K, Aben I, Mckeever J and Frankenberg C 2016 Satellite observations of atmospheric methane and their value for quantifying methane emissions *Atmos. Chem. Phys.* **16** 14371–96

Janardanan R *et al* 2020 Country-scale analysis of methane emissions with a high-resolution inverse model using GOSAT and surface observations *Remote Sens.* **12** 375

Kaiser J *et al* 2012 Biomass burning emissions estimated with a global fire assimilation system based on observed fire radiative power *Biogeosciences* **9** 527–54

Kirschke S *et al* 2013 Three decades of global methane sources and sinks *Nat. Geosci.* **6** 813–23

Kivimaki E *et al* 2019 Evaluation and analysis of the seasonal cycle and variability of the trend from GOSAT methane retrievals *Remote Sens.* **11** 882

Kobayashi S *et al* 2015 The JRA-55 reanalysis: general specifications and basic characteristics *J. Meteorolog. Soc. Japan* **93** 5–48

Lambert G and Schmidt S 1993 Reevaluation of the oceanic flux of methane uncertainties and long-term variations *Chemosphere* **26** 579–89

Lee M, Davis A, Chagunda M and Manning P 2017 Forage quality declines with rising temperatures, with implications for livestock production and methane emissions *Biogeosciences* **14** 1403–17

Lin J and Qian T 2019 A new picture of the global impacts of El Nino-Southern oscillation *Sci. Rep.* **9** 17543

Lyon D *et al* 2015 Constructing a spatially resolved methane emission inventory for the Barnett Shale region *Environ. Sci. Technol.* **49** 8147–57

Maksyutov S *et al* 2013 Regional CO2 flux estimates for 2009–2010 based on GOSAT and ground-based CO2 observations *Atmos. Chem. Phys.* **13** 9351–73

Maksyutov S *et al* 2020 Technical note: a high-resolution inverse modelling technique for estimating surface CO2 fluxes based on the NIES-TM-FLEXPART coupled transport model and its adjoint *Atmos. Chem. Phys. Discuss.* **2020** 1–33

Messie M and Chavez F 2011 Global modes of sea surface temperature variability in relation to regional climate indices *J. Clim.* **24** 4314–31

Miller S *et al* 2013 Anthropogenic emissions of methane in the United States *Proc. Natl Acad. Sci. USA* **110** 20018–22

Miller S, Michalak A, Detmers R, Hasekamp O, Bruhwiler L and Schwietzke S 2019 China's coal mine methane regulations have not curbed growing emissions *Nat. Commun.* **10** 303

MoEFCC 2018 *India: First Biennial Update Report to the UNFCCC* (available at: https://unfccc.int/resource/docs/natc/indbur1.pdf)

Nisbet E *et al* 2019 Very strong. atmospheric methane growth in the 4 years 2014–2017: implications for the Paris agreement *Glob. Biogeochem. Cycles* **33** 318–42

Nisbet E *et al* 2020 Methane mitigation: methods to reduce emissions, on the path to the Paris agreement *Rev. Geophys.* **58** e2019RG000675

Olivier J G J and Peters J A H W 2018 *Trends in Global CO₂ and Total Greenhouse Gas Emissions: 2018 Report* (The Hague: PBL Publishers)

Onogi K *et al* 2007 The JRA-25 reanalysis *J. Meteorolog. Soc. Japan* **85** 369–432

Parker R J *et al* 2020 A decade of GOSAT proxy satellite CH₄ observations *Earth Syst. Sci. Data Discuss.* **2020** 1–36

Parker R, Boesch H, Wooster M, Moore D, Webb A, Gaveau D and Murdiyarso D 2016 Atmospheric CH₄ and CO₂ enhancements and biomass burning emission ratios derived from satellite observations of the 2015 Indonesian fire plumes *Atmos. Chem. Phys.* **16** 10111–31

Patra P, Saeki T, Dlugokencky E, Ishijima K, Umezawa T, Ito A, Aoki S, Morimoto S, Kort E and Crotwell A 2016 Regional methane emission estimation based on observed atmospheric concentrations (2002–2012) *J. Meteorolog. Soc. Japan* **94** 91–113

Peischl J *et al* 2016 Quantifying atmospheric methane emissions from oil and natural gas production in the Bakken shale region of North Dakota *J. Geophys. Res.* **121** 6101–11

Peng S, Piao S, Bousquet P, Ciais P, Li B, Lin X, Tao S, Wang Z, Zhang Y and Zhou F 2016 Inventory of anthropogenic methane emissions in mainland China from 1980 to 2010 *Atmos. Chem. Phys.* **16** 14545–62

Saunois M *et al* 2016a The global methane budget 2000–2012 *Earth Syst. Sci. Data* **8** 697–751

Saunois M *et al* 2017 Variability and quasi-decadal changes in the methane budget over the period 2000–2012 *Atmos. Chem. Phys.* **17** 11135–61

Saunois M *et al* 2020 The global methane budget 2000–2017 *Earth Syst. Sci. Data* **12** 1561–623

Saunois M, Jackson R, Bousquet P, Poulter B and Canadell J 2016b The growing role of methane in anthropogenic climate change *Environ. Res. Lett.* **11** 120207

Scarpelli T, Jacob D, Maasakkers J, Sulprizio M, Sheng J, Rose K, Romeo L, Worden J and Janssens-Maenhout G 2020 A global gridded (0.1 degrees × 0:1 degrees) inventory of methane emissions from oil, gas, and coal exploitation based on national reports to the United Nations framework convention on climate change *Earth Syst. Sci. Data* **12** 563–75

Schleussner C, Rogelj J, Schaeffer M, Lissner T, Licker R, Fischer E, Knutti R, Levermann A, Frieler K and Hare W 2016 Science and policy characteristics of the Paris Agreement temperature goal *Nat. Clim. Change* **6** 827–35

Selvaraju R 2003 Impact of El Nino-southern oscillation on Indian foodgrain production *Int. J. Climatol.* **23** 187–206

Sheng J *et al* 2018a 2010–2016 methane trends over Canada, the United States, and Mexico observed by the GOSAT satellite: contributions from different source sectors *Atmos. Chem. Phys.* **18** 12257–67

Sheng J, Jacob D, Turner A, Maasakkers J, Sulprizio M, Bloom A, Andrews A and Wunch D 2018b High-resolution inversion of methane emissions in the Southeast US using SEAC(4)RS aircraft observations of atmospheric methane: anthropogenic and wetland sources *Atmos. Chem. Phys.* **18** 6483–91

Stohl A, Forster C, Frank A, Seibert P and Wotawa G 2005 Technical note: the Lagrangian particle dispersion model FLEXPART version 6.2 *Atmos. Chem. Phys.* **5** 2461–74

Sun H, Zhou S, Zhang J, Zhang X and Wang C 2020 Year-to-year climate variability affects methane emission from paddy fields under irrigated conditions *Environ. Sci. Pollut. Res.* **27** 14780–9

Tan Z, Zhuang Q, Henze D, Frankenberg C, Dlugokencky E, Sweeney C, Turner A, Sasakawa M and Machida T 2016 Inverse modeling of pan-Arctic methane emissions at high spatial resolution: what can we learn from assimilating satellite retrievals and using different process-based wetland and lake biogeochemical models? *Atmos. Chem. Phys.* **16** 12649–66

Trenberth K, Branstator G, Karoly D, Kumar A, Lau N and Ropelewski C 1998 Progress during TOGA in understanding and modeling global teleconnections associated with tropical sea surface temperatures *J. Geophys. Res.* **103** 14291–324

Troup A 1965 The Southern oscillation *Q. J. R. Meteorolog. Soc.* **91** 490–506

Turner A *et al* 2015 Estimating global and North American methane emissions with high spatial resolution using GOSAT satellite data *Atmos. Chem. Phys.* **15** 7049–69

Turner A, Frankenberg C and Kort E 2019 Interpreting contemporary trends in atmospheric methane *Proc. Natl Acad. Sci. USA* **116** 2805–13

UNFCCC 2020 Greenhouse Gas Inventory Data (available at: https://di.unfccc.int/comparison_by_category)

Wang F *et al* 2019 Methane emission estimates by the global high-resolution inverse model using national inventories *Remote Sens.* **11** 2489

Wang X, Teng F, Zhang J, Khanna N and Lin J 2018 Challenges to addressing non-CO2 greenhouse gases in China's long-term climate strategy *Clim. Policy* **18** 1059–65

Wolter K and Timlin M 2011 El Nino/Southern oscillation behaviour since 1871 as diagnosed in an extended multivariate ENSO index (MEI.ext) *Int. J. Climatol.* **31** 1074–87

Work Resources Institute 2020 Paris Rulebook: global stocktake (Work Resources Institute) (available at: www.wri.org/paris-rulebook/global-stocktake)

Wu X, Zhang X, Chuai X, Huang X and Wang Z 2019 Long-term trends of atmospheric CH₄ concentration across China from 2002 to 2016 *Remote Sens.* **11** 538

Yoshida Y *et al* 2013 Improvement of the retrieval algorithm for GOSAT SWIR XCO2 and XCH4 and their validation using TCCON data *Atmos. Meas. Tech.* **6** 1533–47

Zhang B and Chen G 2014 Methane emissions in China 2007 *Renewable Sustainable Energy Rev.* **30** 886–902

Zhang G, Xiao X, Dong J, Xin F, Zhang Y, Qin Y, Doughty R B and Moore B 2020a Fingerprint of rice paddies in spatial–temporal dynamics of atmospheric methane concentration in monsoon Asia *Nat. Commun.* **11** 554

Zhang Y *et al* 2020b Attribution of the accelerating increase in atmospheric methane during 2010–2018 by inverse analysis of GOSAT observations *Atmos. Chem. Phys. Discuss.* (https://doi.org/10.5194/acp-2020-964)